pH-Mediated Size-Selective Adsorption of Gold Nanoparticles on Diblock Copolymer Brushes

Ye Chan Kim[1], Russell J. Composto[1], and Karen I. Winey[1,2*]*

[1]Department of Materials Science and Engineering, University of Pennsylvania, Philadelphia, Pennsylvania 19104, United States

[2]Department of Chemical and Biomolecular Engineering, University of Pennsylvania, Philadelphia, Pennsylvania 19104, United States

KEYWORDS polymer brushes, block copolymers, nanoparticle adsorption, size separation

ABSTRACT

Precise control of nanoparticles at interfaces can be achieved by designing stimuli-response surfaces that have tunable interactions with nanoparticles. In this study, we demonstrate that a polymer brush can selectively adsorb nanoparticles according to size by tuning the pH of the buffer solution. Specifically, we developed a facile polymer brush preparation method using a symmetric polystyrene-*b*-poly(2-vinylpyridine) (PS-*b*-P2VP) block copolymer deposited on a grafted polystyrene layer. This method is based on the assembly of a PS-*b*-P2VP thin film oriented with parallel lamellar that remains after exfoliation of the top PS-*b*-P2VP layer. We characterized the P2VP brush using X-ray reflectivity and atomic force microscopy. The buffer pH is used to tailor interactions between citrate-coated gold nanoparticles (AuNPs) and the top P2VP block that behaves like a polymer brush. At low pH (~4.0) P2VP brushes are strongly stretched and display a high density of attractive sites, whereas at neutral pH (~6.5) the P2VP brushes are only slightly stretched and have fewer attractive sites. Quartz crystal microbalance with dissipation monitored the adsorption thermodynamics as a function of AuNP diameter (11 and 21 nm) and pH of the buffer. Neutral pH provides limited penetration depth for nanoparticles and promotes size selectivity for 11-nm AuNP adsorption. As proof of concept, the P2VP brushes were exposed to various mixtures of large and small AuNPs to demonstrate selective capture of the smaller AuNPs. This study shows the potential of creating devices for nanoparticle size separations using pH-sensitive polymer brushes.

INTRODUCTION

Understanding the fundamental thermodynamic and dynamic behavior of nanoparticles interacting with surfaces in complex media is essential to advance nanoscale applications that require precise control of nanoparticle transport.[1-4] Of particular interest is the adsorption, desorption, and diffusion dynamics of nanoparticles to surfaces during transport through flow channels or porous gels.[5, 6] Specifically, flow channels reduced to nanoscale maximize the effect of the nanoparticle/channel wall interaction[7, 8] and, thus, it becomes crucial to understand adsorption and desorption behavior of nanoparticles to achieve high-performance nanodevices for separation,[9] purifications,[10] biotherapeutics,[11] and biomimetics[12] applications.

While nanoparticle size, shape, and surface chemistry are important parameters,[13-15] the properties of the surfaces that interact with the nanoparticles also play a critical role in the control of nanoparticle adsorption and desorption on these surfaces, and diffusion through these coatings. There have been many surface modification approaches including chemical treatment,[16, 17] physisorption[18, 19] and topographical patterning.[20, 21] It has been demonstrated that these strategies can be widely employed to control the surface chemistry and functionality that significantly impact wettability, biocompatibility, and antifouling properties. However, for precise control of nanoparticle/surface interactions, the surfaces require more advanced tunability to finely adjust these interactions.

Grafting responsive polymer brushes to surfaces is a promising approach to control surface properties.[22-24] The main advantage of responsive polymer brushes is that their chain conformation and chemistry can be readily controlled using external stimuli. Thus, the interaction between brushes and nanoparticles can be finely tuned by adjusting external conditions (e.g., pH, electric field, and shear stress). Moreover, there are many governing parameters for polymer brushes

including brush thickness, areal number of chains (i.e., grafting density), chemical composition, charge density, charge type (i.e., positive, and negative charge), and crosslinking density. Numerous combinations of external stimuli and these parameters provide expansive opportunities to explore the potential of polymer brushes as functional materials for controlling nanoparticle behavior at interfaces.

The impact of various parameters on the adsorption of nanoparticles to polymer brushes has been widely studied with experiments[25-28] and simulations.[29-31] It has been demonstrated that the areal number of brush chains and brush height are important parameters for governing the thermodynamics of nanoparticle adsorption. Christau *et al.* have suggested that the extent of nanoparticle uptake in a polymer brush highly depends on the brush grafting density and brush thickness.[27, 28] The optimum condition was found for thick brushes with a moderate grafting density (0.2 – 0.3 nm^{-2}) which provides appropriate space for nanoparticles to be absorbed by penetrating into the brush. Thus, nanoparticle adsorption can be controlled by adjusting the brush thickness; nanoparticles form monolayers in thin polymer brushes, while thicker polymer brushes form nanoparticle multilayers with more nanoparticle adsorption.

Based on this understanding, we consider a polymer brush system with tunable nanoparticle adsorption controlled by external stimuli. It is well known that some functional polymers can be protonated, so that transitioning between neutral and charge-containing polymer brushes is possible by controlling the solution pH.[32] As the polymer brush becomes charged, the solvation with water molecules is favored and swelling will ensue.[33, 34] The pH-dependent polymer swelling will control the brush thickness at a fixed polymer molecular weight. This stimuli-responsive polymer brush thickness change has been widely studied for various target applications including dye molecules release[35] and locating nanoparticles in different positions within a

polymer brush for plasmonic applications.[36, 37] These reported studies demonstrate the feasibility of polymer brushes as stimuli-responsive surfaces that adsorb nanoparticles by adjusting the brush thickness and correspondingly the nanoparticle penetration depth.

In this study, we fabricate stimuli-responsive polymer brushes and demonstrate their size selective adsorption of nanoparticles. Purification of nanoparticles based on their size is critical for maximizing the performance of devices requiring monodisperse nanoparticles. While various separation methods have been explored, methods for high degrees of size selectivity are yet to be developed. We first developed a polymer brush fabrication method using a lamellae-forming polystyrene-*b*-poly(2-vinylpyridine) (PS-*b*-P2VP) block copolymer (BCP). Our novel method effectively creates a uniform poly(2-vinylpyridine) (P2VP) brush layer anchored to a grafted polystyrene (gPS) priming layer. The P2VP brushes exhibit pH-dependent swelling in buffer solutions, which imparts control over size-selective nanoparticle adsorption. Quartz crystal microbalance with dissipation (QCM-D) demonstrated pH-dependent size selective adsorption of citrate-coated gold nanoparticles (AuNPs), neutral pH dramatically increased adsorption selectivity for smaller nanoparticles. Using post adsorption atomic force microscope (AFM) and scanning electron microscope (SEM) imaging, the P2VP brush was exposed to binary mixtures of AuNPs to demonstrate that the pH-responsive polymer brush height and the nanoparticle/brush interaction play important roles in controlling the size-selective adsorption of nanoparticles in their mixtures.

RESULTS AND DISCUSSION

Preparation of a Polymer Brush

We present a simple and effective polymer brush preparation process using a lamellae-forming PS-*b*-P2VP with a number average molecular weight (M_n) of 45-*b*-49 kg/mol. The core idea of our design strategy is to create a BCP monolayer of parallel lamellae on a substrate with the PS block on the bottom and the P2VP block on the top. By creating such a structure, the bottom PS remains in a glassy state in various aqueous conditions and rigidly tethers one end of the P2VP chain at the junction between the blocks to achieve a P2VP brush. This is achieved by (1) assembling a BCP lamellar thin film on a gPS layer and (2) exfoliating the excess BCP, leaving only a single lamellae layer with an outer P2VP block (Scheme 1). For the first step, gPS layers were fabricated on a native SiO_2 surface of silicon wafers using a ω-hydroxy-terminated polystyrene (PS-OH) (M_n =18.5 kg/mol), Scheme 1a.[38] Controlling surface energy of native oxide layer of Si wafers with ω-hydroxy-terminated polymers has been demonstrated and widely employed in various studies.[39] In this study, a 5-nm-thick gPS film is formed by spin coating PS-OH onto a silicon oxide surface, followed by thermal annealing and then repeated rinsing with toluene (See the Methods section). This gPS monolayer is covalently bonded to the substrate and presents a hydrophobic surface for subsequent BCP assembly. As demonstrated in Figure S1a, the gPS layers exhibit a smooth (average root-mean-square roughness, R_q = 0.22 nm) and hydrophobic surface (water contact angle, WCA = 88.1°). This hydrophobic nature of the gPS layer provides a thermodynamic driving force for the PS blocks of the BCP to preferentially segregate to the surface during self-assembly. Without the gPS layer, the hydrophilic oxide surface would attract the P2VP domain, resulting in an outer PS domain in the bottom BCP lamellae layer.

The self-assembly of PS-*b*-P2VP parallel lamellar generally yields a PS top surface due to the high surface energy of P2VP.[40, 41] To overcome this surface energy difference, we deposited a thick BCP film on the gPS and then sonicated in methanol to exfoliate the outer layers of the BCP film. This exfoliation step results in a single PS-*b*-P2VP lamellae film with the P2VP at the air/polymer interface. Specifically, a BCP film (45 nm) was thermally annealed on the gPS layer to produce a BCP bilayer, Scheme 1b. As shown in Figure S1b, uniform BCP films with hydrophobic surfaces (PS domain on top) were created after thermal annealing. We note that the WCA of the annealed BCP bilayer thin films (89.5°) are well matched to PS homopolymers (87.9°), indicating the preferential segregation of PS chains to the surface of the BCP bilayers (Figure S1b and S2a). To obtain the P2VP brush at the air/polymer interface (Scheme 1c), methanol was used as a selective solvent for the P2VP block to induce exfoliation of the upper BCP layer. It has been demonstrated that low molecular weight alcohols (e.g., ethanol and methanol) can selectively penetrate and dissolve a domain in self-assembled BCP nanostructures.[42] We found that the initial film thickness (~45 nm) was reduced to ~22 nm after sonication with methanol for 30 min. This reduction of film thickness agrees with AFM height measurements before and after sonicating terraced BCP thin films (Figure S3), wherein sonication with methanol reduced the height without impacting the macroscopic terrace structure. The 50% reduction in film thickness after sonication indicates that sonication with methanol exfoliates the upper BCP lamellar layer to form a P2VP brush.

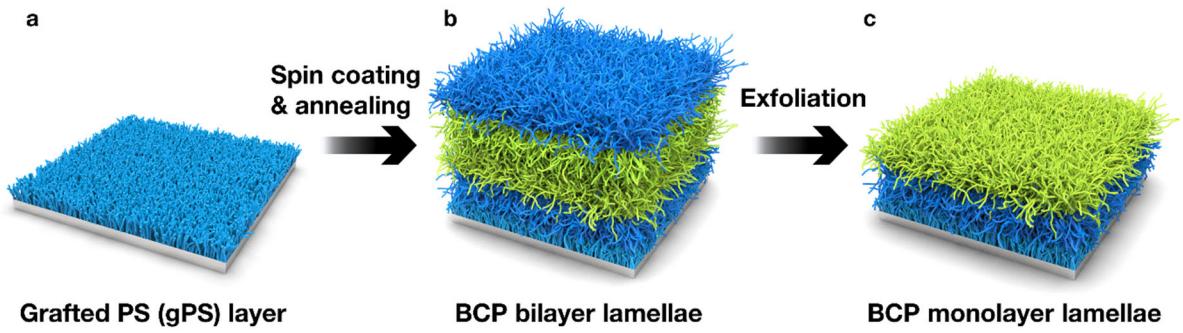

Scheme 1. Illustration of the P2VP brush preparation process on a Si wafer. **(a)** gPS layer fabricated on a Si wafer using PS-OH (light blue). **(b)** BCP bilayer lamellae on gPS layer created using lamellae-forming PS-*b*-P2VP (blue is PS and green is P2VP). **(c)** BCP monolayer lamellae after exfoliation of outer layer.

Characterization of the P2VP Brush Structure

We further demonstrate the formation of a lamellar monolayer with an outer P2VP brush (Figure 1a) by investigating the surface characteristics and the film structure along the out-of-plane direction (z-axis). An AFM height image (Figure 1b) and its profiles (Figure 1c) show that the BCP monolayer has a smooth surface topography with R_q = 0.41 nm. The height profiles obtained for all line scans show deviations between -1 nm and 1 nm, indicating a very uniform surface. Moreover, WCA was observed to be 50° (Figure 1d), which is consistent with the WCA value of P2VP homopolymer films (Figure S2). This indicates that the resulting structure consists of a P2VP top surface with a highly uniform topography, as required for these nanoparticle adsorption studies.

In addition to the characterization of the surface, we investigated the composition profile perpendicular to the film surface using X-ray reflectivity (XRR). As shown schematically in Figure 1e, the expected film structure is a stack of two compositions: a combined PS layer (gPS and PS block) on the bottom and a P2VP brush layer on the top. These PS and P2VP layers have similar electron densities and thus the two layers don't have sufficient contrast for XRR. To address this challenge, the electron density contrast was increased by incorporating gold ions ($AuCl_4^-$) into the P2VP brush as described in the literature[43-45] and Methods section. As shown in Figure 1f, the XRR measurement of the neat BCP monolayer displays the expected oscillations (i.e., Kiessig fringes) associated with the interference of reflections from the top and bottom of the film. In contrast, the reflectivity intensity of the stained BCP monolayer shows additional oscillations characteristic of interference from multiple interfaces.

To determine the thickness of the combined PS layer and the P2VP layer, we utilized a two-layer model to fit the experimental data (black in Figure 1f). As expected, the two layers have

nearly indistinguishable electron densities in the neat BCP monolayer (blue in Figure 1g). The total thickness of the film is 26.4 nm, which is in good agreement with the ellipsometry value. The top surface roughness from the XRR fit is 0.68 nm, which is slightly higher than the value obtained from the AFM height image (0.41 nm), which we attribute to the larger area probed by XRR (~400 mm^2) as compared to AFM (4 μm^2). The electron density profile of the selectively stained BCP monolayer (orange in Figure 1g) shows that the top layer (i.e., stained P2VP) has enhanced electron density. Fitting this reflectivity profile gives 15.8 nm for the combined PS layer thickness and 12.3 nm for the stained P2VP layer thickness. Since the incorporation of the $AuCl_4^-$ increases the P2VP layer thickness, the combined PS layer thickness (15.8 nm) was subtracted from the total thickness of the unstained thin film (26.4 nm) to determine the neat P2VP layer thickness of 10.6 nm.

The grafting density is an important parameter that determines brush characteristics, including brush height and separation. For the BCP system, we use the distance between PS-*b*-P2VP junction points to determine the areal chain number density, σ. Here, σ of the P2VP brush is given by $\sigma = \rho h N_A / M_n$, where ρ is the mass density of the P2VP brush (1.14 g/cm^3), h is brush height (10.6 nm), N_A is Avogadro's number, and M_n is the molecular weight of the P2VP blocks (49 kg/mol). Based on this calculation, the areal chain number density is 0.15 chains/nm^2. Note that the average chain-to-chain distance ($D = \sqrt{1/\sigma}$) is 2.6 nm and much less than $2R_g$ (~10 nm), indicating that the P2VP brush is in the regime exhibits a stretched chain conformation.[46, 47]

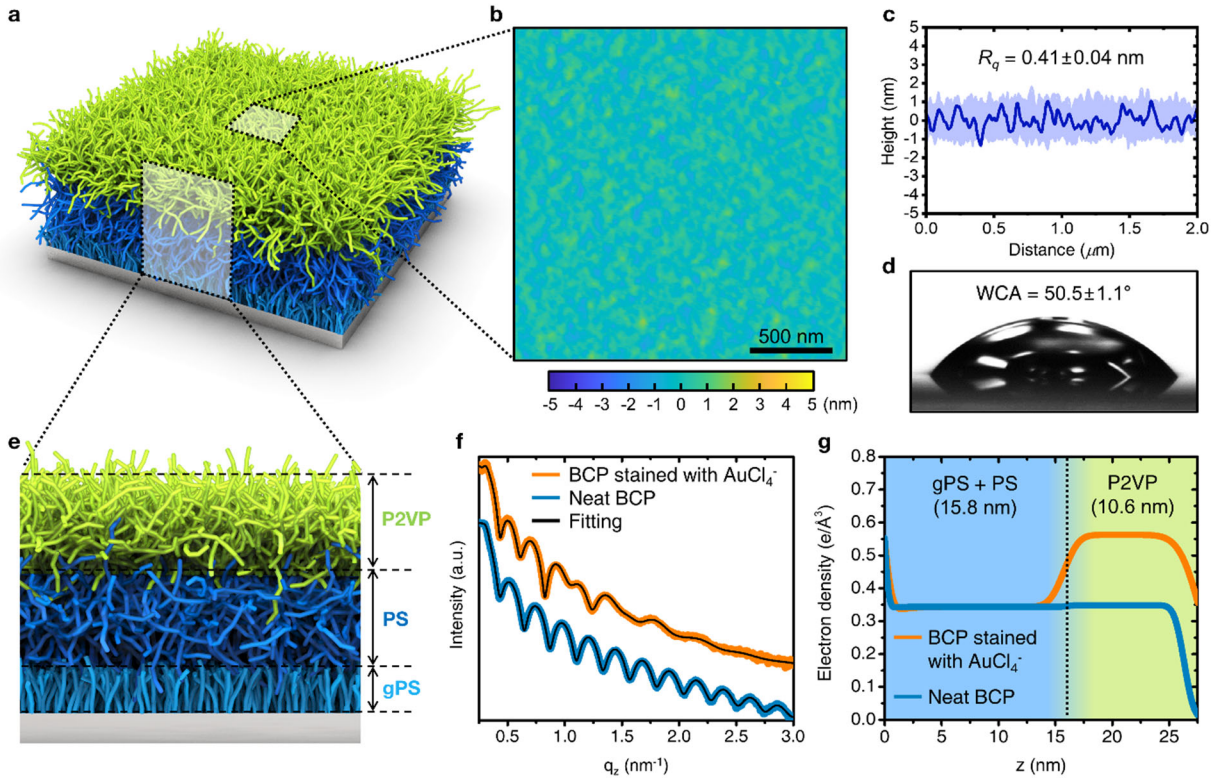

Figure 1. Characterization of P2VP brush using a symmetric PS-*b*-P2VP. (a) Schematic of P2VP brush on a Si wafer (blue is PS and green is P2VP). **(b)** AFM height image (512-by-512 pixels). **(c)** Height profiles collected from every line scan (total 512 lines) are shown in light blue. A representative height profile is shown in blue. **(d)** Photo of a water droplet on the P2VP brush. **(e)** A schematic of the side view of the BCP monolayer. **(f)** X-ray reflectivity profiles and **(g)** the electron density profile along the z-axis of a neat BCP monolayer (blue) and after incorporation of $AuCl_4^-$ ions (orange) in the protonated P2VP brush. The vertical dashed line indicates the position of the junction between the PS and P2VP blocks.

pH Dependence of P2VP Brush

After establishing a facile method to prepare a polar polymer brush, we investigated the pH dependence of the P2VP brush and citrate-coated AuNPs. Because it changes the charge state of the P2VP brush and citrate on the AuNP surface, the pH of the buffer solution can be used to control the thermodynamics and kinetics of AuNP adsorption onto the P2VP brush surface.

First, we investigated the effect of the pH on the P2VP brush height using spectroscopic ellipsometry. Figure 2a shows the in-situ brush height as a function of swelling time for pH values ranging from 6.40 to 3.40. All solutions with different pH values were prepared in 1 mM citrate buffer. The P2VP brush height is obtained by subtracting the combined gPS plus PS domain thickness values from the total film thickness. This approach is valid because the gPS and PS layers are insoluble in the buffer solution whereas only the polar P2VP chains swell. Although P2VP is insoluble in water, the hydrophilicity of P2VP allows water to penetrate into the brush even at pH 6.40. Figure 2a shows that within 1 minute, the P2VP brush thickness increases from 10.6 (dry thickness) to 17.1nm. Decreasing pH to 5.80 and 5.20 results in very slight changes in the brush thickness. Upon decreasing pH further from 4.65 to 4.20 the swollen brush increases significantly from 20nm to 27.5nm. At the lowest pH value of 3.40, the swollen wet brush reaches a thickness of 31.5 nm, a factor of three increase relative to the dry brush. As pH decreases the protonation of the pyridine groups increases causing the P2VP brush chains to absorb water and swell. Because the P2VP blocks are anchored to the glassy PS blocks by covalent bonds, swelling occurs predominately in the out-of-plane direction leading to increased brush thicknesses. At all pH values, the equilibrium thickness is reached in less than 1 minute.

The increase in P2VP brush thickness with decreasing pH is directly related to the degree of P2VP protonation. Thus, we estimate the pK_a of P2VP chains by determining the transition from

a slightly swollen (pH~6.40) to a fully swollen brush (pH~3.40). Figure 2b shows that the equilibrium thickness of the P2VP brush is relatively constant at low pH, decreases sharply and then plateaus above a pH of 5.0. By fitting the thickness with a sigmoidal function, the pK_a of P2VP chains is found to be 4.37 which is in good agreement with other reported values (pK_a~4.5).[48] From this data, we calculate the molar fraction of the ionized group in P2VP chains as shown in Figure 2c (blue) and described in the Supplemental Information (Figure S4a). The pH of the buffer solution controls both the fraction of the ionized group and the wet brush height; a decrease in pH simultaneously leads to the generation of the positively charged group and swelling of brush height. We will use this behavior to control the adsorption of citrate-coated AuNPs onto the P2VP brush surfaces.

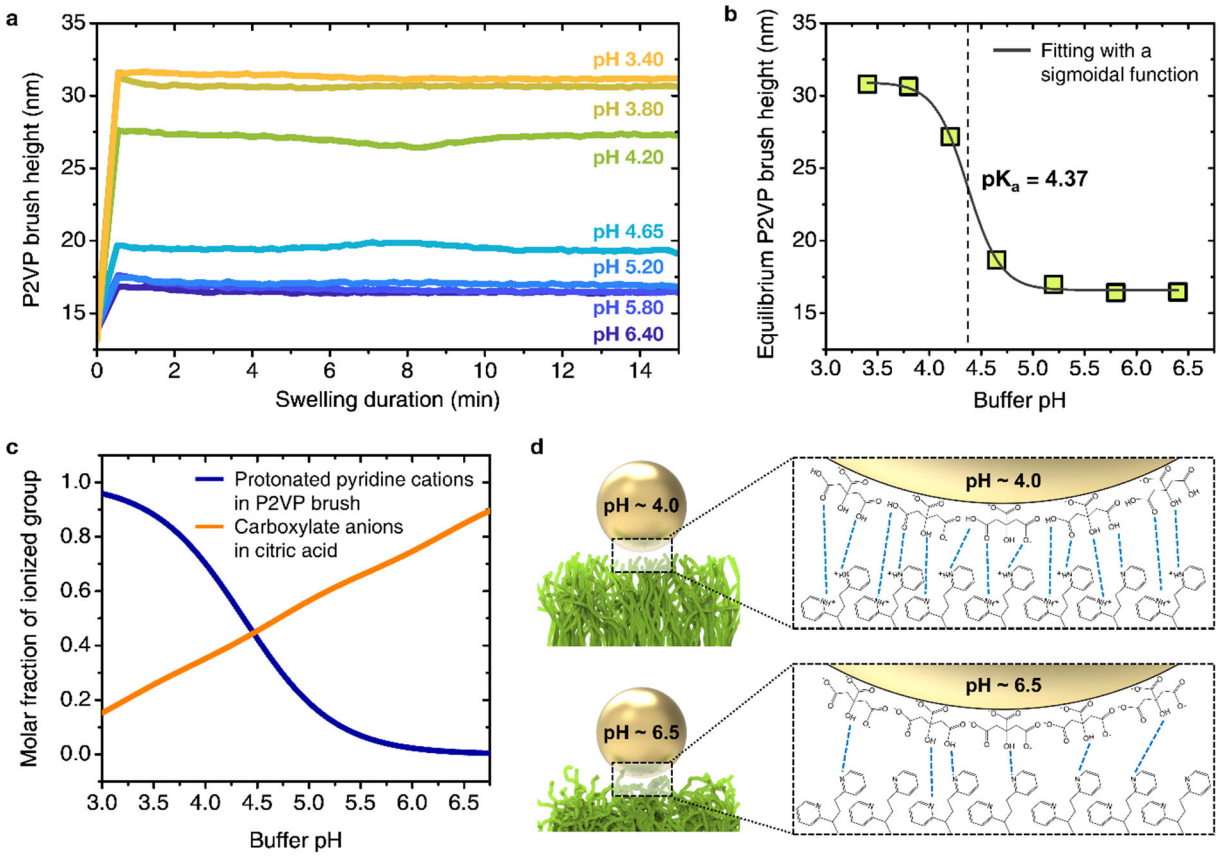

Figure 2. Using pH to control the P2VP brush height and brush interactions with AuNPs. (a) In-situ ellipsometry measurement of P2VP brush thickness and **(b)** equilibrium thickness of P2VP brush as a function of buffer solution pH (1 mM of citrate buffer). **(c)** Theoretically calculated molar fraction of the ionized groups [protonated pyridine cations in P2VP brush and carboxylate anions in citric acid] as a function of pH. **(d)** Schematic of attractive interaction pairs between a citrate-coated AuNP and P2VP brush at pH values of 4.0 and 6.5.

pH Dependence of Interaction Between AuNPs and P2VP Brushes

In addition to tuning the P2VP brush height, the buffer pH also changes the deprotonation of citrate groups on the AuNP surfaces. As demonstrated previously, citric acid exhibits three pK_a values (pK_{a1}=3.13, pK_{a2}=4.76, and pK_{a3}=6.40).[49, 50] From these values, the theoretical molar fraction of each ionized species were calculated as a function of the pH of the buffer solution as shown in Figure S4b. This calculation allows us to estimate the molar fraction of the ionized carboxyl group (COO^-) as described in Supporting Information and presented in Figure 2c (orange). A key characteristic of the AuNP surface and P2VP brush is that the fraction of the ionized carboxyl groups monotonically increases as the pH increases whereas the fraction of cationic pyridine groups on the P2VP brush decreases as pH increase, respectively. As a result of this complementary behavior, the solution pH provides sensitive control over the interactions between AuNPs and P2VP surface.

Electrostatic and hydrogen bonding are the two main interactions that dictate the adsorption strength of citrate-coated AuNPs onto the P2VP brush. Using the known molar fraction of ionized groups, we can estimate relative strengths of the electrostatic attraction and hydrogen bonding between the AuNP and P2VP. Figure 2c shows that the electrostatic attraction between the citrate coated AuNPs and the P2VP brush exhibits a maximum value near pH~4.5. At pH values greater or less than this value, there are more ionized carboxyl or pyridine groups, respectively, resulting in weaker electrostatic interactions. On the other hand, for hydrogen bonding, a variety of bonding combinations are available even when the pH is below 4.5 (excess of ionized pyridine), whereas above 4.5 the number of combinations is reduced; see Supporting Information and Figure S5.

In summary, Figure 2d shows a detailed representation of the interfacial interactions between the AuNPs and the P2VP brush. Representative pH values below and above the cross-

over (pH 4.0 and 6.5) exhibit the different types of interactions present under these conditions. At pH 4.0, brush conformation is highly stretched (~30 nm) and as a result the P2VP exposes many attractive ionized pyridine sites allowing for both electrostatic and hydrogen bonding between the citrate and P2VP brush. In contrast, at pH 6.5, the brush conformation is weakly stretched (~16 nm) and presents fewer surface sites resulting in fewer electrostatic bonds as well as no hydrogen bonding.

pH-Mediated AuNP Adsorption

Based on the understanding of the pH-mediated interactions presented in the prior section, we investigated the adsorption behavior of AuNPs onto P2VP brushes at pH values below and above the crossover (pH 4.0 and 6.5). Specifically, two AuNPs were studied with diameters of 11 nm and 21 nm to investigate how the pH-mediated adsorption of AuNPs varies depending on the particle size. The average diameter, D, of the citrate-coated AuNPs and the polydispersity index (PDI) were determined by fitting form factors to transmission small angle X-ray scattering (Tr-SAXS) data (Figure S6). No small q dependence is observed in the form factor of AuNPs, consistent with a good dispersion.

The stability of 11-nm and 21-nm AuNPs at two pH values was further investigated by measuring the zeta potential and UV-Vis-NIR spectra (Table S1 and Figure S7). To ensure the stable binding of citrate ligands on the AuNP surface, 1 mM citrate buffer was used for all experiments to maintain an excess of citrate within the solution. As expected, AuNPs exhibit sufficient negative zeta potential (< -10 mV) in all cases, which ensures a stable dispersion. A single extinction peak in the UV-Vis-NIR spectra is observed for all cases (11-nm and 21-nm AuNPs at pH 4.0 and pH 6.5), clearly supporting the AuNP stability. We note that the absolute

zeta potential values at pH 6.5 are higher than at pH 4.0, which is consistent with the theoretical predictions of charge fraction of citrate groups in the previous section.

After we demonstrated the AuNP stability at pH 4.0 and 6.5, AuNP adsorption to the P2VP brush was observed by QCM-D measurements. We used SiO_2 coated QCM sensors and the P2VP brush was prepared by following the same procedure used for ellipsometry studies. Note that the preparation of the P2VP brush was successful on the QCM sensors, even though bare QCM sensors are rougher than Si wafers (Figure S8).

To measure the AuNP adsorption we monitored the changes in resonance frequency, Δf_n, with various overtones (n = 3, 5, 7, and 9) while flowing a dilute AuNP suspension over the P2VP brush. Having demonstrated that our QCM-D data of AuNP adsorption to the P2VP brush can be modelled using the Sauerbrey equation[51] (See the Method section and Figure S9), we use Δf_n to compute the areal mass of AuNPs as a function of time. The areal number of adsorbed AuNPs was calculated by dividing the areal mass by the mass of one AuNP. Figure 3a and 3b show the increase and saturation of adsorbed AuNPs at pH 4.0 and 6.5, respectively, for 11-nm and 21-nm AuNPs. As demonstrated in Figure 2d, the low pH buffer solution stretches the P2VP brush, increasing the number of attractive interactions between the partially charged P2VP brush and citrate-coated AuNPs. This condition induces both the 11-nm and 21-nm AuNPs to adsorb into the P2VP brush (Figure 3a). At pH 4.0, the swollen brush height was measured to be 31.5 nm, and the AuNPs penetrate the brush, as confirmed with SEM and AFM images after adsorption (Figures 3c and 3d). The adsorbed AuNPs appeared to overlap in the SEM image (11-nm AuNPs) and in the AFM height image (21-nm AuNPs). Figure 3e is a schematic of the adsorbed and stacked AuNPs in the P2VP brush at low pH. Notably, at a fixed pH, the number of adsorbed AuNPs depends on particle

size. The number of AuNPs required to fill the permeable space inside the brush is greater when the particles are small. Thus, the brush provides more capacity for smaller nanoparticle adsorption.

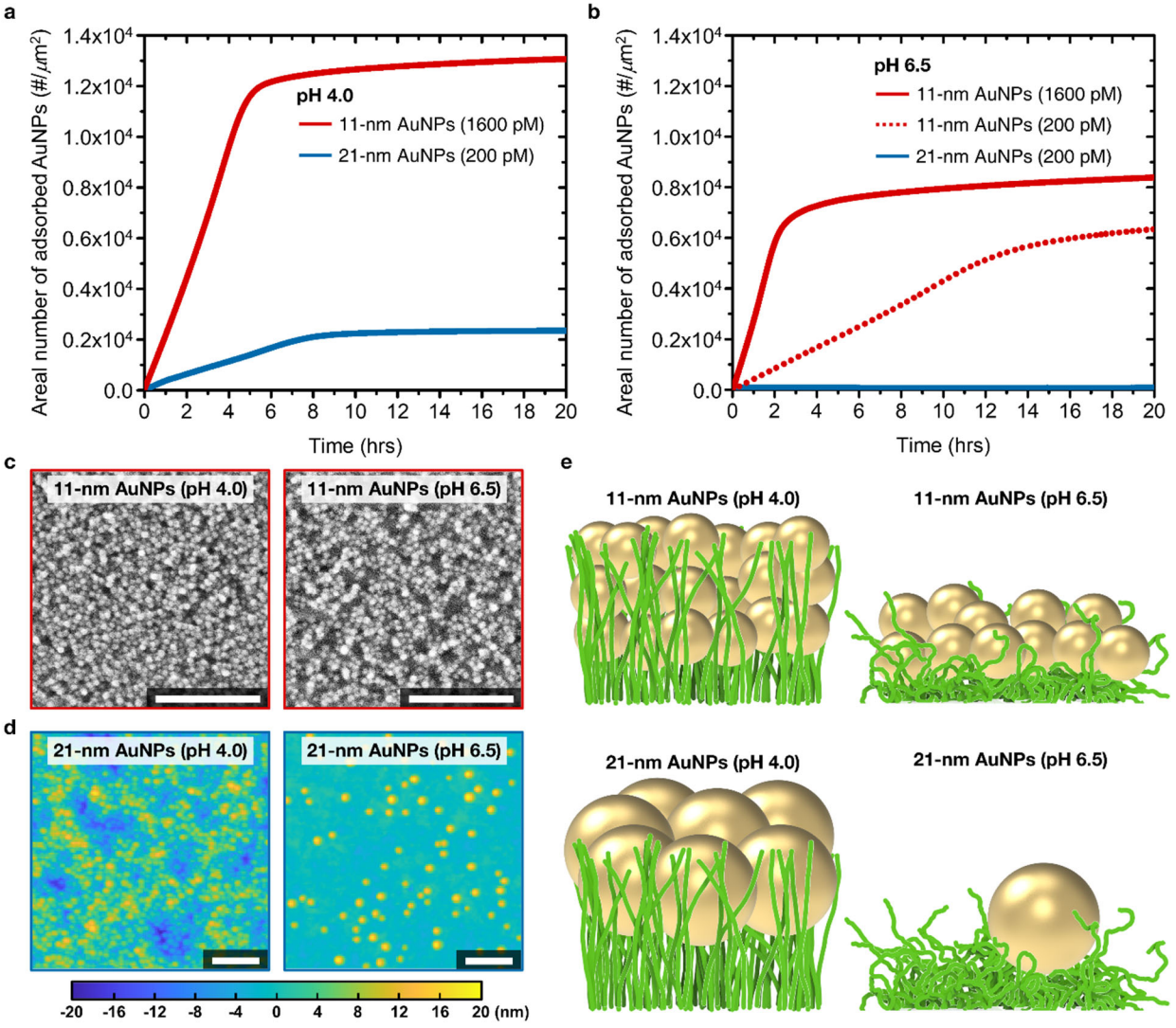

Figure 3. pH-mediated AuNPs adsorption to the P2VP brush. The real-time areal number of adsorbed AuNPs with diameters of 11 nm (red) and 22 nm (blue) in 1 mM citrate buffer of **(a)** pH 4.0 and **(b)** pH 6.5. **(c)** SEM images (11-nm AuNPs) and **(d)** AFM height maps (22-nm AuNPs) after adsorption at pH 4.0 and pH 6.5 for 20 hrs. **(e)** Schematic of adsorbed AuNPs depending on pH and particle size. Scale bars in (c) and (d) are 200 nm.

Remarkably, this size-dependent adsorption is even more pronounced at neutral pH. At pH 6.5, the P2VP brush is less swollen (~16 nm) and presents fewer attractive sites compared to the acidic condition, pH 4.0. The penetration of the larger nanoparticles into a more compact and less ionized brush is greatly reduced relative to the smaller nanoparticles. By contrast, the 11-nm AuNPs adsorb at pH 6.5 to a considerable areal number density (~8500 μm^{-2}, Figure 3b). The small AuNPs are capable of penetrating into the brush, and accordingly, the total number of interactions between the P2VP brush and the AuNPs is increased to enable adsorption of the particles. Relative to acidic conditions (pH 4.0), the total areal number of 11-nm AuNPs at neutral conditions is lower by 35%. In contrast, the adsorption of 21-nm AuNPs at pH 6.5 is very sparse (~80 μm^{-2}) exhibiting a 96% decrease relative to acidic conditions. This behavior is attributed to the larger particle diameter compared to the brush height and the fewer number of ionized sites. Both contributions result in a reduction of the 21-nm AuNPs adsorbing onto the P2VP brush in the neutral condition. While adsorbed 11-nm AuNPs are crowded and form a multilayer at pH 6.5 (Figure 3c), the adsorbed 21-nm AuNPs lie in one plane and are sell separated. This sparse sub-monolayer of 21-nm AuNPs reflects both the impenetrable P2VP brush at neutral pH and the weak NP-brush interactions. We demonstrate that this significant size-dependent AuNP adsorption on P2VP brushes cannot be attributed to a difference in the molar concentration of the nanoparticle suspension (1600 pM of 11-nm AuNPs and 200 pM of 21-nm AuNPs). As shown in Figure 3b, the adsorption of 11-nm and 21-nm AuNPs at the same concentration, 200 pM, still shows higher adsorption for the small nanoparticles, indicating that the molar concentration of AuNPs affects primarily adsorption kinetics. As expected, adsorption kinetics of 11-nm AuNPs at 1600 pM is much faster than that of 11-nm AuNPs at 200 pM. Adsorption kinetics as a function of nanoparticle concentration, size, and pH will be investigated by follow-up studies.

To sum up, as schematically shown in Figure 3e, buffer pH effectively controls the adsorption of AuNPs in P2VP brushes. At low pH (~4.0), the P2VP brush is highly stretched with sufficient ionization sites to promote AuNP adsorption regardless of particle size. In contrast, at neutral pH (~6.5) less brush swelling and weaker NP-P2VP interactions result in moderate adsorption of the small nanoparticles and negligible adsorption of the large nanoparticles. We note that the absolute zeta potential of 11-nm AuNPs is less than that of 21-nm AuNPs (Table S1), which implies fewer citrate ligands on the smaller particles. The selective adsorption of smaller particles, despite having fewer interaction sites than larger particles, indicates the importance of nanoparticle penetration into the polymer brush to maximize the nanoparticle/polymer brush contacts. This behavior at neutral pH suggests that the P2VP brush can be used to separate large and small AuNPs.

Size-Selective Adsorption from Binary Mixtures of AuNPs

We further investigate the ability of the P2VP brush to selectively adsorb AuNPs from binary mixtures of large and small nanoparticles. The AuNP binary mixtures were prepared by mixing 1 mM citrate buffer solution and AuNPs solutions so that the volume of each mixture is 3 mL, the concentration of the 21-nm AuNPs is fixed at 200 pM and the concentration of the 11-nm AuNPs is varied (100, 200, 300, and 400 pM). The P2VP brush was prepared on a Si wafer and then diced into 1×5 cm^2 pieces and immersed in the binary mixtures of AuNPs. As demonstrated in Figure 3b, the maximum capacity of the P2VP brush for adsorption of 11-nm AuNPs at pH 6.5 is ~8500 μm^{-2}. Thus, the P2VP brush area of 1×5 cm^2 provides sufficient capacity (~4×10^{12} of 11-nm AuNPs) to uptake every 11-nm AuNPs even in the highest concentration of 400 pM (~7.2×10^{11} of 11-nm AuNPs).

The objective of this study is to demonstrate that the smaller NPs can be selectively removed from a mixture of large and small nanoparticles. The performance of the P2VP brush as a size-selective adsorber was investigated at pH 4.0 and 6.5. At pH 4.0 and 6.5, the AuNPs mixtures with 1:1 molar ratio (200 pM of 11-nm AuNPs and 200 pM of 21-nm AuNPs) is chosen as representative examples in Figure 4a, 4b, and 4c, and 4d, 4e and 4f, respectively.

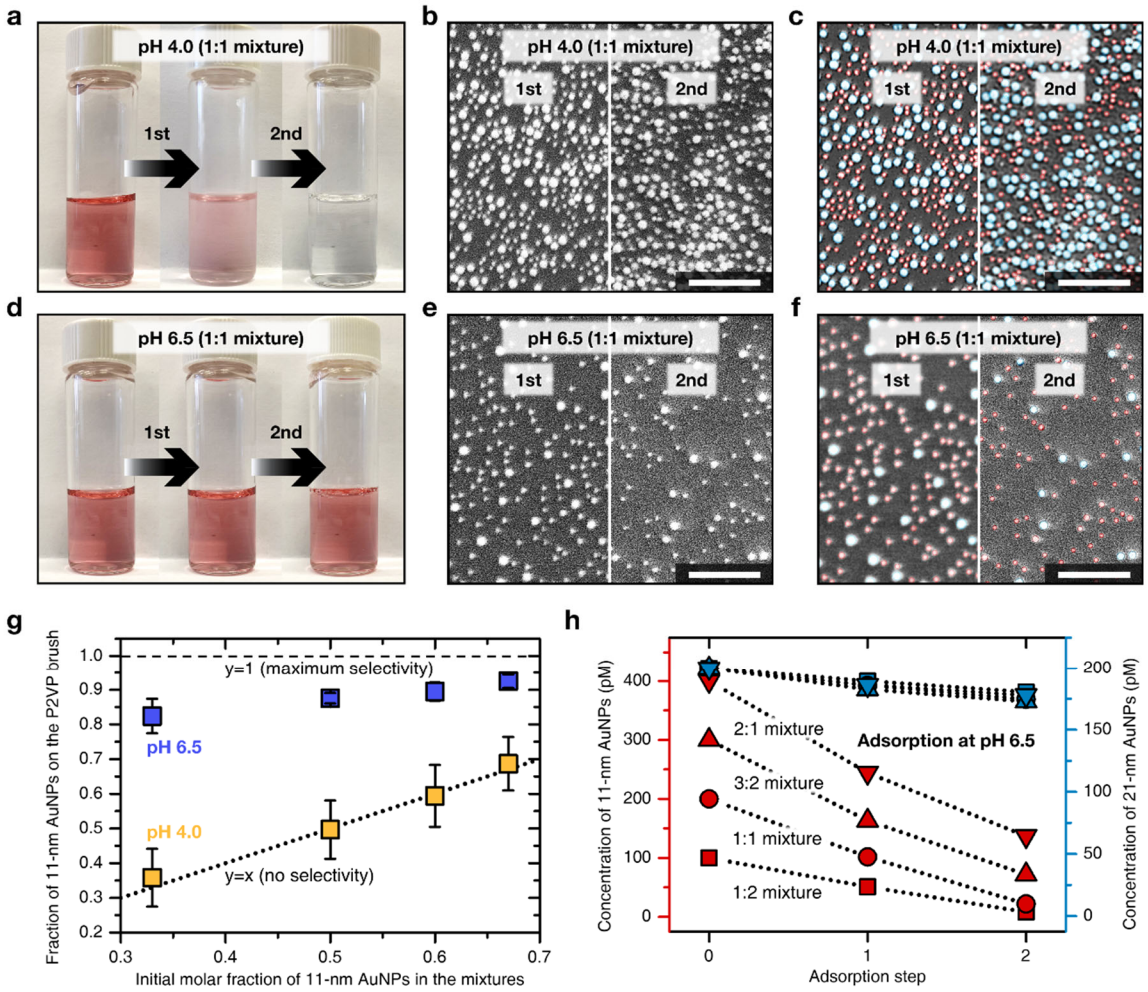

Figure 4. pH-mediated size selective adsorption of AuNPs to P2VP brush from binary mixtures of nanoparticles. (a, d) Photos of AuNPs binary mixtures, **(b, e)** raw SEM images and **(c, f)** analyzed SEM images indicate the size of the adsorbed AuNPs (11 nm, red, 21 nm, blue) after 1st and 2nd adsorption from the 1:1 AuNP mixture at pH 4.0 (upper panel) and pH 6.5 (bottom panel). **(g)** Size selectivity for 11-nm AuNPs as a function of nanoparticle mixing ratios in the initial suspensions and pH. **(h)** Calculated concentrations of AuNP suspensions after the 1st and 2nd adsorption processes at pH 6.5. Scalebars in (b), (c), (e), and (f) are 200 nm.

At pH 4.0, the initial red color of the AuNP solution becomes pale pink after the adsorption for 7 days (1st adsorption, Figure 4a). The change in solution color from red to pink implies a decrease in the overall AuNP concentration. To investigate the possibility of complete removal of AuNPs, we facilitate the AuNP adsorption kinetics by inserting a fresh wafer coated with the P2VP brush (1×5 cm^2). As shown in Figure 4a, the AuNP solution color becomes clear after the 2nd 7-day exposure using a fresh P2VP brush. This is consistent with removal of most of the AuNPs from solution and attributed to NP adsorption at pH 4.0, which is insensitive to nanoparticle size. The number and size of adsorbed AuNPs was quantified by SEM image analysis (Figure 4b and 4c). The image processing method of SEM images is described in Figure S10. After the 1st adsorption, due to the faster adsorption kinetics of small particles, the fraction of adsorbed 11-nm AuNPs is slightly more than 50%. After the 2nd adsorption, most of the remaining particles were adsorbed, so that the fraction of adsorbed 11-nm AuNPs is a little less than 50%. The solution becomes clear and the total ratio of adsorbed 11-nm and 21-nm AuNPs after 1st and 2nd adsorption steps reaches the mixing ratio of the initial solution (1:1), indicating that low pH (~ 4.0) equally removes the small and large AuNPs from the mixed solutions and is an ineffective condition for size separation.

However, for pH 6.5, the AuNP mixture solution exhibits no color change after the 1st and the 2nd 7-day adsorption (Figure 4d). In the concentration range of prepared mixtures (<400 pM), the red color is predominantly due to the 21-nm AuNPs because 11-nm AuNPs show much lower extinction coefficient. This observation suggests that the concentration of 21-nm AuNPs remains relatively constant after the two adsorption steps on the P2VP brush. To verify the selective adsorption of 11-nm AuNPs onto the P2VP brush at pH 6.5, we again quantify the number and size of AuNPs adsorbed using SEM image analysis (Figure 4e and 4f). As we expected, the number

fraction of adsorbed 11-nm AuNPs reaches ~90%, which is much higher than the initial molar fraction of 11-nm AuNPs in the mixture (~50%). The solution color remains red indicating that most of 21-nm AuNPs remain in the solution at pH 6.5, while the 11-nm AuNPs are predominantly adsorbed onto the P2VP brush. These immersion studies demonstrate that neutral pH (~6.5) is an effective condition for separating smaller AuNPs from the mixture.

The pH-dependent size-selective adsorption of AuNPs onto the P2VP brush is also investigated as a function of the initial mixing ratio of AuNPs (Figure 4g). As described above, we fixed 21-nm AuNP concentration at 200 pM and varied 11-nm AuNP concentrations in the range from 100 pM to 400 pM, so that there are four mixing fractions of 11-nm AuNPs (0.33, 0.5, 0.6, and 0.67). Detailed studies from a mixture with a molar fraction of 0.5 were presented in Figures 4a-f. The fraction of adsorbed 11-nm AuNPs are calculated by summing both the first and second adsorption steps. At pH 4.0, the fraction of adsorbed 11-nm AuNPs strongly depends on the mixing ratio of 11-nm and 21-nm AuNPs and agrees with the molar fraction of the suspension (dotted line, Figure 4g) indicating no preferential adsorption based on NP size. By contrast, at pH 6.5, adsorption of the 11-nm AuNPs is strongly favored and increases slightly with mixing ratio from 82% to 92%, as the molar fraction increases from 0.33 to 0.67, respectively.

To further quantify this preference for adsorbing the small AuNPs at neutral conditions, we estimated the number of AuNPs remaining in the suspension. The concentration of residual AuNPs was estimated by subtracting the number of AuNPs adsorbed to the P2VP brush from the initial number of AuNPs in the binary mixture solutions (Figure 4h). As the number of adsorption steps increases, the concentration of the 11-nm AuNPs is greatly reduced at all molar fractions, while the concentration of 21-nm AuNPs is slightly reduced. For example, when suspensions that initially contain 200 pM of both nanoparticles undergo two adsorption steps, the final

concentrations of the 21-nm and 11-nm AuNPs are ~ 175 pM and ~ 22 pM, respectively. These results clearly demonstrate size selective adsorption of 11-nm AuNPs to the P2VP brush at pH 6.5 from a binary mixture of NPs. Furthermore, the extent of this adsorption can be increased by increasing the lateral area of P2VP brush.

CONCLUSIONS

Here, we demonstrated that size selective adsorption of AuNPs to a P2VP brush depends on pH of the buffer solution. First, we devised a facile fabrication method for brush preparation using a BCP. The formation of bilayer lamellar thin films followed by the exfoliation of the upper layer effectively creates a BCP brush monolayer on the Si wafer and QCM-D crystal surfaces with the polar P2VP block exposed to the surface. This developed method does not include complex and expensive chemical modification for polymer brush grafting, thus, suitable for scale-up the manufacturing process. AFM and XRR measurements were performed to characterize the P2VP brush structures, which are highly uniform P2VP brush across surface with a dry thickness of 10.6 nm. The pH-dependent response of the P2VP brush thickness was measured with in-situ ellipsometry and varied from 16.5 to 30.8 nm as pH decreased from 6.40 to 3.40, respectively. The molar fractions of ionic and non -ionic species in P2VP and citrate molecules were determined as a function of pH and this information was used to establish the interactions between citrate-coated AuNPs and the P2VP brush. Based on our understanding of brush swelling and NP-brush interactions, nanoparticle adsorption was studied at two representative pH values pH 4.0 and pH 6.5. At pH 4.0, there is sufficient swelling of the P2VP brush with many available interaction sites with the citrate-coated AuNPs, while pH 6.5 produces limited swelling of P2VP brush with fewer interaction sites. Using in-situ QCM-D, AuNPs adsorption was measured for 11-nm and 21-nm

AuNPs. Size selective adsorption for the smaller 11-nm AuNPs is maximized when the penetration of large 21-nm AuNPs is limited, namely at neutral pH. We further demonstrated the potential application of P2VP brushes for size selective NP separation using suspensions containing 11-nm and 21-nm NP sizes, wherein the 11-nm AuNPs were preferentially adsorbed at pH = 6.5. Overall, this study provides a strong foundation upon which to build technologies for nanoparticle size separations using pH sensitive polymer brushes. Furthermore, the underlying physics of selective adsorption revealed in this study may not be limited to spherical AuNPs and has the potential to improve separation and purification techniques for nanoparticles with different shape and type, biological particles (e.g., bacteria and viruses), and molecules.

METHODS

Materials

A symmetric PS-*b*-P2VP with a M_n of 45-*b*-49 kg/mol (PDI=1.07) and a PS-OH with a M_n of 18.5 kg/mol (PDI=1.01) were purchased from Polymer Source. The citric acid (>99.5%), sodium citrate tribasic dihydrate (>99%), gold(III) chloride trihydrate ($HAuCl_4 \cdot 3H_2O$, >99.9%), and suspensions of gold nanoparticles (AuNPs) were purchased from Sigma Aldrich.

P2VP brush preparation

Si wafers and QCM sensors were used as substrates for brush preparation, and they were rinsed with toluene and subjected to a UV-ozone cleaning process before use. PS-OH and PS-*b*-P2VP were dissolved in toluene at 1.5 wt.% and 1.7 wt%, respectively, and passed through a syringe filter before use. To create the gPS layer, a PS-OH solution was spin-coated onto the substrates at a spin speed of 1500 rpm for 60 s to produce ~50 nm thick films. The PS-OH thin films were thermally annealed at 160 °C under a vacuum for 24 hrs to produce chemical bonds between the

hydroxy groups on the SiOx layer of the substrates and the PS-OH chains. The unreacted residual PS-OH chains were removed by soaking in toluene for 3 hrs, and the gPS layers were measured to have a thickness of ~6 nm. PS-*b*-P2VP was spin-coated directly on the gPS layers, and the spin speed was carefully adjusted around 3000 rpm to have a thickness of ~45 nm. BCP thin films on the gPS layers were thermally annealed at 170 °C under vacuum for 24 hrs to create a bilayer of parallel lamellae. Sonication of the thermally annealed BCP thin films in methanol for 30 min induced exfoliation of the upper layer, resulting in a P2VP top brush surface of monolayer parallel lamellar.

Incorporation of gold precursor in P2VP brush

To enhance the electron density contrast between PS and P2VP chains for XRR experiments, protonation of P2VP chains (cations) and selective incorporation of $AuCl_4^-$ (anions) into protonated P2VPs were simultaneously performed by soaking the samples in a 5 mM $HAuCl_4$/3wt% HCl solution for 3 hrs.[43-45] Subsequent rinsing with deionized water and blown with N_2 gas was conducted.

XRR and Tr-SAXS experiments

XRR and Tr-SAXS experiments were performed using the Dual-source and Environmental X-ray Scattering facility at the University of Pennsylvania. The data were collected using a GeniX3D beam source (8 keV, Cu Kα, wavelength=1.54 Å) and a PILATUS 1 M detector. In the case of XRR, the sample size is 30×50 mm^2 and the beam size is 8×0.17 mm^2, and data were measured at a 363-mm sample-to-detector distance by changing the angle of incidence from 0° to 2° at 0.002° intervals for 60 s. The XRR data were analyzed utilizing the REFLEX software.[52] In the case of Tr-SAXS, AuNP solutions were placed in 1.5 mm diameter glass capillaries and measured. To

obtain data over a wide q-range, data were obtained at sample-to-detector distance of 363 mm and 2520 mm and combined.

In-situ monitoring of brush thickness

In-situ observation of the brush thickness according to the pH value of the buffer solution was performed using a custom-made liquid chamber mounted on an ellipsometry (J.A. Woollam Co., alpha-SE). A sample was placed in the chamber and fixed using tape. After adding 20 mL of 1-mM citrate buffer solution at a specific pH, thickness was monitored as a function of time at 10 s intervals.

Characterization of AuNP stability

Zeta potentials of AuNPs were measured by Delsa Nano C (Beckman Coulter). The citrate-coated 11-nm and 21-nm AuNPs were dispersed in 1 mM citrate buffer solutions at pH 4.0 and pH 6.5, and transferred to a disposable cell for the measurements. AuNP stability was also characterized by UV-Vis-NIR spectroscopy (Varian Cary 5000 UV-Vis-NIR spectrophotometer).

QCM-D experiments

SiO_2 (50 nm) coated QCM-D sensors were purchased from Nanoscience Instruments (Qsensors QSX 303). The brush preparation on the QCM sensors was the same as described above. All QCM-D monitoring measurements were performed using a Q-sense Analyzer instrument at 21.0 °C. The flow rate of AuNP solutions was fixed at 200 μL/min. QCM-D measures changes of the resonance frequency of QCM sensors, Δf_n, where n (n=1, 3, 5, …) is the number of the harmonics. Theoretically, this change of frequency is directly related to the mass of the adsorbed AuNPs, so that Δf_n provides the accumulated mass of the AuNP adsorbed to the brush. Ideally, Δf_n and the mass obey the Sauerbrey equation, $\frac{\Delta f_n}{n} = -\frac{2f_0^2}{\sqrt{\rho_q \mu_q}}\frac{\Delta m}{A}$, where the f_0 is the fundamental frequency,

ρ_q is the physical density of quartz, μ_q is the shear modulus of quartz crystal, Δm is the mass change, and A is active crystal area.[51] This relation assumes the formation of rigid and thin layers that couple with the quartz crystal. To confirm the applicability of the Sauerbrey equation to our system, we monitored the changes in resonance frequency with various overtones (n = 3, 5, 7, and 9) during the AuNP adsorption. The overtones overlap in all cases (Figure S9), thus confirming the formation of rigid adsorbed layers. Also, the maximum change of frequency is < 0.025% of the initial resonant frequency, which further confirms the formation of a rigid and thin layer.

AFM imaging

AFM (Dimension Icon AFM, Bruker) was used in tapping mode with probes (HQ:NSC15/Al BS, MikroMasch) that have a resonance frequency of 325 kHz, a force constant of 40 N/m, and a radius of 8 nm. For image scanning, the scan rate, integral gain, proportional gain, and amplitude setpoint were set to 1.00 Hz, 1.20, 6.00, and 550 mV, respectively.

SEM imaging

SEM (JEOL 7500F) was utilized to collect images of adsorbed AuNPs in P2VP brush. The operation energy was 5 keV, and the working distance was 5 mm.

ASSOCIATED CONTENT

Supporting Information

The Supporting Information is available free of charge

Surface characterization of gPS layer and BCP bilayer and monolayer lamellae; Water contact angle of PS and P2VP homopolymer thin films; Top layer exfoliation of macroscopically terraced BCP bilayer lamellae; Molar fraction of each species and ionized groups depending on the pH; Interactions between P2VP and citrate-coated AuNPs depending on the pH; Characterization of AuNPs size by small angle X-ray scattering; Characterization of AuNP stability by zeta potential and UV-Vis-NIR spectra; Preparation of P2VP brush on the QCM sensors; Monitoring frequency change during the AuNP adsorption with various overtones; Image processing of SEM images to calculate the fraction of AuNPs (PDF)

AUTHOR INFORMATION

Corresponding Authors

Russell J. Composto - Department of Materials Science and Engineering, University of Pennsylvania, Philadelphia, Pennsylvania 19104, United States

Email: composto@seas.upenn.edu

Karen I. Winey - Department of Chemical and Biomolecular Engineering and Department of Materials Science and Engineering, University of Pennsylvania, Philadelphia, Pennsylvania 19104, United States

Email: winey@seas.upenn.edu

Authors

Ye Chan Kim - Department of Materials Science and Engineering, University of Pennsylvania, Philadelphia, Pennsylvania 19104, United States

Author Contributions

R.J.C and K.I.W initiated and supervised the project. Y.C.K principally performed all experiments and data analysis. Y.C.K prepared figures and manuscript, and R.J.C and K.I.W revised the draft.

Notes

The authors declare no competing financial interests.

ACKNOWLEDGMENT

R.J.C., K.I.W., and Y.C.K. acknowledge funding by the NSF-CBET-2034122. The authors acknowledge use of the Dual Source and Environmental X-ray Scattering facility operated by the Laboratory for Research on the Structure of Matter at the University of Pennsylvania (NSF MRSEC 17-20530). The equipment purchase was made possible by a NSF MRI grant (17-25969), a ARO DURIP grant (W911NF-17-1-0282), and the University of Pennsylvania. The authors also gratefully acknowledge Prof. Daeyeon Lee for supporting QCM-D experiments.

REFERENCES

(1) Chen, P.; Huang, Z.; Liang, J.; Cui, T.; Zhang, X.; Miao, B.; Yan, L.-T. Diffusion and directionality of charged nanoparticles on lipid bilayer membrane. *ACS Nano* **2016**, *10* (12), 11541-11547.
(2) Jamali, V.; Hargus, C.; Ben-Moshe, A.; Aghazadeh, A.; Ha, H. D.; Mandadapu, K. K.; Alivisatos, A. P. Anomalous nanoparticle surface diffusion in LCTEM is revealed by deep learning-assisted analysis. *Proc. Natl. Acad. Sci. U.S.A.* **2021**, *118* (10), e2017616118.
(3) Kang, S.; Kim, J.-H.; Lee, M.; Yu, J. W.; Kim, J.; Kang, D.; Baek, H.; Bae, Y.; Kim, B. H.; Kang, S. Real-space imaging of nanoparticle transport and interaction dynamics by graphene liquid cell TEM. *Sci. Adv.* **2021**, *7* (49), eabi5419.
(4) Babayekhorasani, F.; Dunstan, D. E.; Krishnamoorti, R.; Conrad, J. C. Nanoparticle diffusion in crowded and confined media. *Soft Matter* **2016**, *12* (40), 8407-8416.
(5) Dettmer, S. L.; Pagliara, S.; Misiunas, K.; Keyser, U. F. Anisotropic diffusion of spherical particles in closely confining microchannels. *Phys. Rev. E* **2014**, *89* (6), 062305.
(6) Wang, D.; Wu, H.; Liu, L.; Chen, J.; Schwartz, D. K. Diffusive escape of a nanoparticle from a porous cavity. *PRL* **2019**, *123* (11), 118002.
(7) Sidhu, I. S.; Frischknecht, A. L.; Atzberger, P. J. Electrostatics of Nanoparticle–Wall Interactions within Nanochannels: Role of Double-Layer Structure and Ion–Ion Correlations. *ACS Omega* **2018**, *3* (9), 11340-11353.
(8) Mojarad, N.; Krishnan, M. Measuring the size and charge of single nanoscale objects in solution using an electrostatic fluidic trap. *Nat. Nanotechnol.* **2012**, *7* (7), 448-452.
(9) Gaborski, T. R.; Snyder, J. L.; Striemer, C. C.; Fang, D. Z.; Hoffman, M.; Fauchet, P. M.; McGrath, J. L. High-performance separation of nanoparticles with ultrathin porous nanocrystalline silicon membranes. *ACS Nano* **2010**, *4* (11), 6973-6981.
(10) Sweeney, S. F.; Woehrle, G. H.; Hutchison, J. E. Rapid purification and size separation of gold nanoparticles via diafiltration. *J. Am. Chem. Soc.* **2006**, *128* (10), 3190-3197.
(11) Mitchell, M. J.; Billingsley, M. M.; Haley, R. M.; Wechsler, M. E.; Peppas, N. A.; Langer, R. Engineering precision nanoparticles for drug delivery. *Nat. Rev. Drug Discov.* **2021**, *20* (2), 101-124.
(12) Amin Arefi, S.; Tony Yang, C. W.; Sin, D. D.; Feng, J. J. Simulation of nanoparticle transport and adsorption in a microfluidic lung-on-a-chip device. *Biomicrofluidics* **2020**, *14* (4), 044117.
(13) Park, J.; Bailey, E. J.; Composto, R. J.; Winey, K. I. Single-particle tracking of nonsticky and sticky nanoparticles in polymer melts. *Macromolecules* **2020**, *53* (10), 3933-3939.
(14) Albanese, A.; Tang, P. S.; Chan, W. C. The effect of nanoparticle size, shape, and surface chemistry on biological systems. *Annu. Rev. Biomed. Eng.* **2012**, *14* (1), 1-16.
(15) Rose, K. A.; Gogotsi, N.; Galarraga, J. H.; Burdick, J. A.; Murray, C. B.; Lee, D.; Composto, R. J. Shape Anisotropy Enhances Nanoparticle Dynamics in Nearly Homogeneous Hydrogels. *Macromolecules* **2022**.
(16) Pujari, S. P.; Scheres, L.; Marcelis, A. T.; Zuilhof, H. Covalent surface modification of oxide surfaces. *Angew. Chem. Int. Ed.* **2014**, *53* (25), 6322-6356.
(17) Shave, M. K.; Zhou, Y. T.; Kim, J.; Kim, Y. C.; Hutchison, J.; Bendejacq, D.; Goulian, M.; Choi, J.; Composto, R. J.; Lee, D. Zwitterionic surface chemistry enhances detachment of bacteria under shear. *Soft Matter* **2022**, *18* (35), 6618-6628. DOI: 10.1039/d2sm00065b.
(18) Durning, C.; O'shaughness, B.; Sawhney, U.; Nguyen, D.; Majewski, J.; Smith, G. Adsorption of poly (methyl methacrylate) melts on quartz. *Macromolecules* **1999**, *32* (20), 6772-6781.

(19) Koga, T.; Jiang, N.; Gin, P.; Endoh, M. K.; Narayanan, S.; Lurio, L. B.; Sinha, S. K. Impact of an Irreversibly Adsorbed Layer on Local Viscosity of Nanoconfined Polymer Melts. *PRL* **2011**, *107* (22), 225901. DOI: 10.1103/PhysRevLett.107.225901.
(20) Chen, D.; McKinley, G. H.; Cohen, R. E. Spontaneous wettability patterning via creasing instability. *Proc. Natl. Acad. Sci. U.S.A.* **2016**, *113* (29), 8087-8092. DOI: doi:10.1073/pnas.1522700113.
(21) Lee, J. A.; McCarthy, T. J. Polymer surface modification: Topography effects leading to extreme wettability behavior. *Macromolecules* **2007**, *40* (11), 3965-3969.
(22) Chen, W.-L.; Cordero, R.; Tran, H.; Ober, C. K. 50th anniversary perspective: Polymer brushes: Novel surfaces for future materials. *Macromolecules* **2017**, *50* (11), 4089-4113.
(23) Li, D.; Xu, L.; Wang, J.; Gautrot, J. E. Responsive polymer brush design and emerging applications for nanotheranostics. *Adv. Healthc. Mater.* **2021**, *10* (5), 2000953.
(24) Stuart, M. A. C.; Huck, W. T.; Genzer, J.; Müller, M.; Ober, C.; Stamm, M.; Sukhorukov, G. B.; Szleifer, I.; Tsukruk, V. V.; Urban, M. Emerging applications of stimuli-responsive polymer materials. *Nat. Mater.* **2010**, *9* (2), 101-113.
(25) Kesal, D.; Christau, S.; Trapp, M.; Krause, P.; von Klitzing, R. The internal structure of PMETAC brush/gold nanoparticle composites: a neutron and X-ray reflectivity study. *Phys. Chem. Chem. Phys.* **2017**, *19* (45), 30636-30646. DOI: 10.1039/c7cp04404f.
(26) Filippidi, E.; Michailidou, V.; Loppinet, B.; Ruhe, J.; Fytas, G. Brownian diffusion close to a polymer brush. *Langmuir* **2007**, *23* (9), 5139-5142. DOI: 10.1021/la0637162.
(27) Christau, S.; Möller, T.; Yenice, Z.; Genzer, J.; von Klitzing, R. Brush/gold nanoparticle hybrids: effect of grafting density on the particle uptake and distribution within weak polyelectrolyte brushes. *Langmuir* **2014**, *30* (43), 13033-13041.
(28) Christau, S.; Thurandt, S.; Yenice, Z.; Von Klitzing, R. Stimuli-responsive polyelectrolyte brushes as a matrix for the attachment of gold nanoparticles: The effect of brush thickness on particle distribution. *Polymers* **2014**, *6* (7), 1877-1896.
(29) Zhang, Q. Y.; Xiang, X. Adsorption of a spherical nanoparticle in polymer brushes: Brownian dynamics investigation. *Phys. A: Stat. Mech. Appl.* **2013**, *392* (18), 3857-3862. DOI: 10.1016/j.physa.2013.05.001.
(30) Cheng, S. F.; Stevens, M. J.; Grest, G. S. Ordering nanoparticles with polymer brushes. *J. Chem. Phys.* **2017**, *147* (22). DOI: 10.1063/1.5006048.
(31) Etha, S. A.; Pial, T. H.; Das, S. Extensive Stable Physical Contacts between a Nanoparticle and a Highly Repulsive Polymeric Layer. *J. Phys. Chem. B* **2022**, *126* (30), 5715-5725. DOI: 10.1021/acs.jpcb.2c04010.
(32) Geoghegan, M. Weak polyelectrolyte brushes. *Soft Matter* **2022**, *18* (13), 2500-2511.
(33) Geoghegan, M.; Ruiz-Pérez, L.; Dang, C. C.; Parnell, A. J.; Martin, S. J.; Howse, J. R.; Jones, R. A.; Golestanian, R.; Topham, P. D.; Crook, C. J. The pH-induced swelling and collapse of a polybase brush synthesized by atom transfer radical polymerization. *Soft Matter* **2006**, *2* (12), 1076-1080.
(34) Ferrand-Drake del Castillo, G.; Emilsson, G.; Dahlin, A. Quantitative analysis of thickness and pH actuation of weak polyelectrolyte brushes. *J. Phys. Chem. C* **2018**, *122* (48), 27516-27527.
(35) Kumar, S.; Dory, Y. L.; Lepage, M.; Zhao, Y. Surface-grafted stimuli-responsive block copolymer brushes for the thermo-, photo-and pH-sensitive release of dye molecules. *Macromolecules* **2011**, *44* (18), 7385-7393.

(36) Roiter, Y.; Minko, I.; Nykypanchuk, D.; Tokarev, I.; Minko, S. Mechanism of nanoparticle actuation by responsive polymer brushes: from reconfigurable composite surfaces to plasmonic effects. *Nanoscale* **2012**, *4* (1), 284-292.
(37) Tokareva, I.; Minko, S.; Fendler, J. H.; Hutter, E. Nanosensors based on responsive polymer brushes and gold nanoparticle enhanced transmission surface plasmon resonance spectroscopy. *J. Am. Chem. Soc.* **2004**, *126* (49), 15950-15951.
(38) Lee, H.; Sethuraman, V.; Kim, Y.; Lee, W.; Ryu, D. Y.; Ganesan, V. Nonmonotonic Glass Transition Temperature of Polymer Films Supported on Polymer Brushes. *Macromolecules* **2018**, *51* (12), 4451-4461. DOI: 10.1021/acs.macromol.8b00290.
(39) Mansky, P.; Liu, Y.; Huang, E.; Russell, T.; Hawker, C. Controlling polymer-surface interactions with random copolymer brushes. *Science* **1997**, *275* (5305), 1458-1460.
(40) Hu, H.; Gopinadhan, M.; Osuji, C. O. Directed self-assembly of block copolymers: a tutorial review of strategies for enabling nanotechnology with soft matter. *Soft Matter* **2014**, *10* (22), 3867-3889.
(41) Kim, Y.; Yong, D.; Lee, W.; Ahn, H.; Kim, J. H.; Kim, J. U.; Ryu, D. Y. Order-to-Disorder Transition of Lamella-Forming PS-b-P2VP Films Confined between the Preferential Surface and Neutral Substrate. *Macromolecules* **2019**, *52* (22), 8672-8681.
(42) Miller-Chou, B. A.; Koenig, J. L. Dissolution of symmetric diblock copolymers with neutral solvents, a selective solvent, a nonsolvent, and mixtures of a solvent and nonsolvent monitored by FT-IR imaging. *Macromolecules* **2003**, *36* (13), 4851-4861.
(43) Kim, Y. C.; Shin, T. J.; Hur, S. M.; Kwon, S. J.; Kim, S. Y. Shear-solvo defect annihilation of diblock copolymer thin films over a large area. *Sci. Adv.* **2019**, *5* (6), eaaw3974.
(44) Kim, Y. C.; Kim, S. Y. A Single Crystal 2D Hexagonal Array in a Centimeter Scale with a Self-Directed Assembly of Diblock Copolymer Spheres. *ACS Nano* **2022**, *16* (3), 3870-3880.
(45) Chai, J.; Wang, D.; Fan, X.; Buriak, J. M. Assembly of aligned linear metallic patterns on silicon. *Nat. Nanotechnol.* **2007**, *2* (8), 500-506.
(46) Brittain, W. J.; Minko, S. A structural definition of polymer brushes. *J. Polym. Sci. A Polym. Chem.* **2007**, *45* (16), 3505-3512.
(47) Neubauer, N.; Winkler, R.; Tress, M.; Uhlmann, P.; Reiche, M.; Kipnusu, W. K.; Kremer, F. Glassy dynamics of poly (2-vinyl-pyridine) brushes with varying grafting density. *Soft Matter* **2015**, *11* (15), 3062-3066.
(48) Tantavichet, N.; Pritzker, M. D.; Burns, C. M. Proton uptake by poly (2-vinylpyridine) coatings. *J. Appl. Polym. Sci.* **2001**, *81* (6), 1493-1497.
(49) Grys, D. B.; de Nijs, B.; Salmon, A. R.; Huang, J. Y.; Wang, W. T.; Chen, W. H.; Scherman, O. A.; Baumberg, J. J. Citrate Coordination and Bridging of Gold Nanoparticles: The Role of Gold Adatoms in AuNP Aging. *ACS Nano* **2020**, *14* (7), 8689-8696. DOI: 10.1021/acsnano.0c03050.
(50) Martin, R. B. A COMPLETE IONIZATION SCHEME FOR CITRIC ACID. *J. Phys. Chem.* **1961**, *65* (11), 2053-2055. DOI: 10.1021/j100828a032.
(51) Sauerbrey, G. Verwendung von Schwingquarzen zur Wägung dünner Schichten und zur Mikrowägung. *Z. Phys.* **1959**, *155* (2), 206-222. DOI: 10.1007/BF01337937.
(52) Vignaud, G.; Gibaud, A. REFLEX: a program for the analysis of specular X-ray and neutron reflectivity data. *J. Appl. Crystallogr.* **2019**, *52* (1), 201-213.

For Table of Contents Only